
This is an electronic reprint of the original article.
This reprint may differ from the original in pagination and typographic detail.

Venkatasubramanian, Sathya; Li, Linsheng; Lehtovuori, Anu; Icheln, Clemens; Haneda, Katsuyuki

Impact of using resistive elements for wideband isolation improvement

Published in:
IEEE Transactions on Antennas and Propagation

DOI:
[10.1109/TAP.2016.2630727](https://doi.org/10.1109/TAP.2016.2630727)

Published: 18/11/2016

Document Version
Peer-reviewed accepted author manuscript, also known as Final accepted manuscript or Post-print

Please cite the original version:
Venkatasubramanian, S., Li, L., Lehtovuori, A., Icheln, C., & Haneda, K. (2016). Impact of using resistive elements for wideband isolation improvement. *IEEE Transactions on Antennas and Propagation*, 65(1), 52-62. <https://doi.org/10.1109/TAP.2016.2630727>

This material is protected by copyright and other intellectual property rights, and duplication or sale of all or part of any of the repository collections is not permitted, except that material may be duplicated by you for your research use or educational purposes in electronic or print form. You must obtain permission for any other use. Electronic or print copies may not be offered, whether for sale or otherwise to anyone who is not an authorised user.

Impact of using resistive elements for wideband isolation improvement

Sathya N. Venkatasubramanian, Linsheng Li, Anu Lehtovuori, Clemens Icheln and Katsuyuki Haneda

Abstract—Improving the isolation between antenna elements in compact arrays has been a major focus of recent research. In this paper, we present ideas to improve the wideband isolation between closely spaced antennas. We do this by connecting lumped lossy (resistive) elements between the antenna feeds. A simple analytical expression is provided to compute the impact of resistive elements on efficiency to analyse the power lost in the resistive element. Three configurations of decoupling circuits are designed and fabricated for two closely spaced monopoles operating at 2.4 GHz. The decoupling circuit contains transmission lines of different lengths at the antenna inputs such that the mutual admittance between the antenna elements is 1) resistive, 2) resistive and inductive, or 3) resistive and capacitive. Lumped elements are then connected between the transmission lines followed by matching circuit. The paper shows that with configurations 2) and 3) we can improve the wideband isolation compared to 1), as well as compared to using only lossless elements. The wideband isolation was improved by 17.6 dB across a 200 MHz band at 2.4 GHz, with a final isolation level of 20 dB over that band. Better than 30 dB isolation was achieved across a narrower band of 55 MHz. The proposed technique provides wideband isolation improvement for multiple-input multiple-output (MIMO) as well as narrowband performance with large isolation suitable for in-band full-duplex (FDX) applications. The impact on efficiency is investigated to verify that the advantages from the improved wideband isolation outweighs the possible reduction in overall efficiency.

Index Terms—antenna, decoupling, isolation, MIMO, full-duplex.

I. INTRODUCTION

THE rapid penetration of wireless systems has resulted in increased demand for high data rate, low latency systems to provide quality wireless access to the end user. Over the past decade, various techniques have been used to increase the throughput like multiple-input multiple-output (MIMO) and other multi-antenna techniques. Individual radio frequency signals at multi-antenna ports are decorrelated either by increasing the isolation between two antennas, or by using antennas with dissimilar radiation patterns. This results in

Manuscript received April 26, 2016; revised September 27, 2016; accepted November 07, 2016.

S. N. Venkatasubramanian, A. Lehtovuori, C. Icheln and K. Haneda are with Dept. of Radio Science and Engineering, Aalto University School of Electrical Engineering, Espoo, Finland. L. Li was with Dept. of Radio Science and Engineering, Aalto University School of Electrical Engineering, Espoo, Finland until July 2016. Since Aug. 2016 he is with the research center of Huawei in Helsinki, Finland.

The research work leading to these results was funded by the Academy of Finland, under the project (In-band Full-Duplex MIMO Transmission: A Breakthrough to High-Speed Low-Latency Mobile Networks), and the Finnish Funding Agency for Technology and Innovation, Tekes, under the project (Full-Duplex Cognitive Radio: Technology and Application to Cognitive M2M Communications) and the Aalto ELEC doctoral school, Finland.

spatial diversity and multiplexing, thus improving the channel capacity in MIMO transmission. One of the major aspects in the design of multi-element antenna arrays in compact devices is the inter-element spacing between the antenna elements. A reasonably large spacing has to be maintained to achieve a low enough level of correlation between the antennas [1], while it is desired to implement as many antennas as possible within a limited space. Hence, antenna isolation has been given significant attention in recent years due to its impact on decoupling multi-antenna elements.

Also, in-band full-duplex (FDX) radio transmission is an attractive solution for improving the link throughput. This requires the transmit (Tx) and receive (Rx) antennas to be isolated sufficiently in order to cancel the self-interference (SI) by its own transmission with additional analog and digital cancellation techniques [2], [3]. The radio frequency (RF) decoupling circuit decreases the SI sufficiently to prevent saturation of the Analog-to-Digital Converter (ADC) at the receiver. The major challenge in implementing compact bi-directional FDX devices is the requirement of significantly larger Tx-Rx isolation levels compared to those in MIMO systems. In single antenna solutions described in [4], [5], the isolation between the Tx and Rx ports connected to a common antenna element is of the order of 20 dB; the isolation is ensured using a circulator, which also increases the cost of the device. Many other FDX transceivers consider separating the Tx and Rx antennas far apart to improve antenna isolation. For example, an FDX transceiver [5] uses co-polarized commercial Tx and Rx antennas that are separated by 30 cm to achieve port isolation of 27 dB at 2.4 GHz. Their antenna designs have an unacceptable antenna footprint for compact devices. Therefore, a novel antenna design is required to accomplish a comparable isolation level with much smaller footprint.

Various techniques have been used to improve isolation and decrease the correlation between antenna elements of an array with very small spacing between elements as discussed in [6] and references therein. Many techniques have been proposed to improve isolation in a compact antenna array, but usually they do not consider wideband isolation improvement. In order to improve the port-to-port isolation for wideband systems, various methods have been proposed. In the neutralization technique [7], transmission lines are connected at certain locations between the antennas to improve the isolation. Lumped elements connected between the antenna feeds, with transmission lines of specific length from the antenna inputs can also be used to improve the port-to-port isolation [6], [8], [9]. Other methods propose to use a combination of reactive elements; e.g. [10] implements an LC-

TABLE I
SUMMARY OF ACHIEVED ISOLATION WITH RELATIVE BANDWIDTH FOR
EXISTING TECHNIQUES.

Previous work	Relative bandwidth		
	15 dB	20 dB	25 dB
Isolation level	15 dB	20 dB	25 dB
Diallo et al. [7]	11.4%	5.7%	3.4%
Chen et al. [8]	2.2%	1.1%	0.8%
Wu et al. [9]	5.95%	5.1%	1.7%
Zhao et al. [6]	19%	15%	4%
Bhatti et al. [10]	1.7%	0.7%	0.2%
Tang et al. [14]	3.1%	1%	0%
Tang et al. [17]	1.6%	0.4%	0%
Krewski et al. [18]	4.1%	1.5%	0%
Mak et al. [21]	4%	1.8%	0.8%
Valkonen et al. [22]	2.7%	0%	0%
Proposed method	20.8%	7.9%	4.3%

based branchline coupler at the input of a two-element antenna array at 710 MHz achieving narrowband isolation of 20 dB across 4 MHz bandwidth. Furthermore, decoupling networks are designed based on different techniques like the eigenmode theory in [11]–[15] and characteristic mode theory [16]. In [17], [18], a decoupling and matching network is proposed based on even-odd mode analysis. [17], [19], [20] discuss improving dual-band isolation using lumped elements between the antenna feeds. Mak in [21] proposes a field cancellation element to artificially create a coupling path to improve the antenna isolation. For effective comparison of already existing techniques, Table I lists the achieved relative bandwidth for a given isolation level between closely spaced antennas. It should be noted that this comparison does not take into account the original isolation and size of the antenna system. However, none of these methods provide enough wideband isolation for FDX operation, e.g., 30 dB isolation over at least 2% bandwidth at 2.4 GHz while [6] achieves 25 dB isolation across 4% relative bandwidth. Therefore, novel wideband antenna decoupling methods are needed.

One promising solution for realizing wideband isolation in compact antenna arrays is the use of resistive elements [23]. However, the losses of the resistive elements may decrease the total efficiency of the antenna array. In this paper, the impact of using a resistive element on efficiency is studied, supported by an analytical expression of the losses introduced by a resistive element between the antenna feeds. Three different configurations of decoupling circuits are designed for two closely spaced monopoles that are implementable in a compact device. The decoupling circuit comprises of transmission lines connected to the antenna feeds followed by a lossy decoupling circuit. By adjusting the lengths of transmission lines, the mutual admittance between the two antennas can be transformed to purely real, or real with positive or negative imaginary parts as seen from the junction with the decoupling network. The measured prototypes are compared with a reference prototype of two closely spaced monopoles without any isolation improvement, demonstrating 30 dB and 20 dB of isolation for the relative bandwidth of 2.2% and 7.8% respectively.

The proposed decoupling technique is applicable both to MIMO and FDX applications, improving the wideband isola-

tion for MIMO as well as isolation levels significantly over a narrower bandwidth for FDX applications. The improvement often comes at the cost of some power lost in the cancellation circuit. One of the main benefits of the proposed method is the enhanced ability to the mentioned improvement compared to the existing methods, due to the use of both the resistive and reactive components in the decoupling circuit. For example, LTE Band 7 and the 2.4 GHz ISM band have a relative bandwidth of 7.2% with 4.1% respectively, which is quite large compared to isolation provided by most existing methods in Table I. Improvement in the wideband isolation can result in improved efficiency as well as reduction of the spatial correlation due to coupling thereby affecting MIMO link performance. In case of FDX applications for relaying, significantly larger levels of isolation are required [2] to suppress the self-interference to the noise level of the receiver, improving the link throughput. Our decoupling circuits are one of the essential enabler of the FDX transceiver by decreasing the SI at the RF stage and prevent the receiver ADCs from being saturated due to the interference.

In summary, the main contributions of this paper are

- Demonstrating the use of resistive along with reactive elements between antenna feeds to improve the wideband isolation; this idea was introduced in the authors' previous manuscript [23], but now the idea is significantly strengthened using analytical and experimental analysis.
- Providing a simple analytical expression to compute the impact of the resistive elements on efficiency, which can be used to analyse the trade-off between isolation and efficiency; and finally,
- Validation by prototyping and measurements, and demonstration of the decoupling for compact antenna arrays.

The content of this article is organized as follows. Section II gives theoretical background of the proposed decoupling technique using resistive elements. Formulas for analysing the impact of the lossy elements on total efficiency of the antenna system are also given. In Section III, the proposed decoupling method is numerically analysed to illustrate the improvement in wideband isolation. Having described the prototypes of the proposed decoupling network and validated their performance against numerical evaluation in Section IV, Section V concludes the paper.

II. THEORETICAL BACKGROUND

A. Proposed decoupling method

In this section, the theoretical background of the proposed decoupling network using resistive elements for improving the wideband isolation is discussed. The benefit of using resistive and combination of both resistive and reactive elements between the antenna feeds is shown analytically.

Consider a two-port network represented by its S parameters, S_{ij} , and admittance parameters, Y_{ij} . A two-element antenna array can be represented in the form of a π -network, with the mutual admittance Y_{21} between the two antennas denoting the mutual coupling as shown in Fig. 1(a). It can thus be inferred that cancelling the mutual admittance ($-Y_{21}$) with

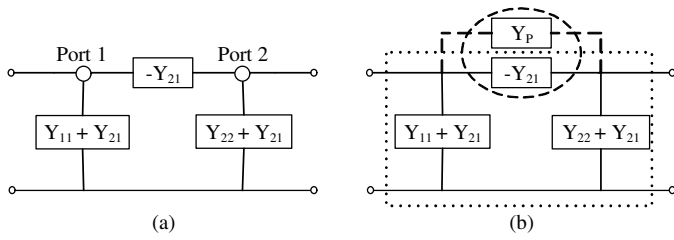


Fig. 1. (a) Two-port network with Y parameters and (b) Two-port network with additional parallel element.

a parallel element with admittance Y_P results in improved port-to-port isolation, as depicted in Fig. 1(b). The box indicated by dotted lines shows the two-port representation of the antenna and the dashed curve denotes the mutual coupling and the compensating element. As the two port network is symmetric, the circuit can be analysed as two circuits with even and odd mode inputs [24], allowing us to obtain an insight on the wideband performance of the decoupling circuit. From basic microwave theory, the S parameters of a two port network can be decomposed into even and odd mode components [25] as

$$S_{11} = \frac{1}{2}(S_{11}^{\text{even}} + S_{11}^{\text{odd}}) \quad \text{and} \quad S_{21} = \frac{1}{2}(S_{11}^{\text{even}} - S_{11}^{\text{odd}}).$$

Thus, in order to achieve high total isolation, the even and odd mode admittances should fulfill $S_{11}^{\text{even}} = S_{11}^{\text{odd}}$. This implies that the even and odd mode admittances should also be equal. The even and odd mode input admittances of a general two port network are given by

$$Y_{11}^{\text{even}} = Y_{11} + Y_{21} \quad \text{and} \quad Y_{11}^{\text{odd}} = Y_{11} - Y_{21}. \quad (1)$$

When a parallel element is connected between the inputs, the even and odd mode admittances as shown in Fig. 2 become

$$Y_{11}^{\text{even}} = Y_{11} + Y_{21} \quad \text{and} \quad Y_{11}^{\text{odd}} = Y_{11} - Y_{21} + 2Y_P, \quad (2)$$

where Y_P refers to the admittance of the parallel element connected between the antenna feeds. The phase of the antenna mutual admittance can be transformed to a different value by adding transmission lines at the input before connecting the parallel element. This enables us to use different combinations of elements for the cancellation circuit as the real and imaginary components of the mutual admittance vary with phase. For ease of understanding, the transmission lines are not explicitly shown in the figures and considered as a part of the antenna, i.e. they are included in Y_{11} and Y_{21} .

Previous works such as [9], [22], [26] improve the input matching and antenna decoupling simultaneously, but they tend to result in a narrowband solution. Fig. 2 shows that the added parallel element does not impact the even mode admittance but only the odd mode. Hence, depending on the value of Y_{21} at the centre frequency of the design, the odd mode admittance is increased by $2Y_P$ such that $Y_{11}^{\text{even}} = Y_{11}^{\text{odd}}$.

In [8], it is shown that connecting a single reactive element between the two antennas improves the isolation at the centre frequency. That was made possible by adding transmission lines of a specific length beneath the antenna ports such that the mutual admittance of the antenna becomes purely imaginary. The main limitation of this method is the bandwidth over

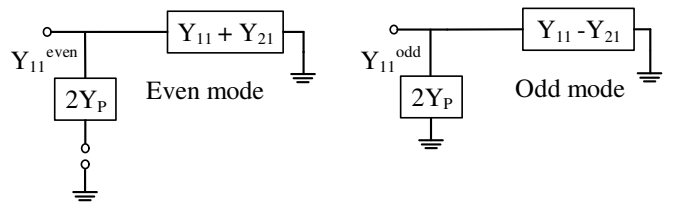


Fig. 2. Even and odd mode admittances of two port network with a parallel element.

which high isolation can be achieved; the mutual admittance at frequencies on either side of the centre frequency will have a resistive component, where $-\Re\{Y_{21}\}$ can be positive. This requires a negative resistance for cancellation as $\Re\{Y_P\} < 0$ which requires active elements for implementation.

As discussed in [23], when we assume the antennas to be perfectly matched at the design frequency, i.e. $|S_{11}| = |S_{22}| = 0$ before adding the decoupling circuit, and reciprocal, i.e. $S_{21} = S_{12}$, the mutual admittance is given by

$$Y_{21} = Y_0 \frac{-2S_{21}}{1 - S_{21}^2}. \quad (3)$$

Approximating the above expression, and assuming that the magnitude of $S_{21} \ll 1$, the term S_{21}^2 in the denominator can be neglected, thus yielding

$$Y_{21} \approx -2Y_0 S_{21}. \quad (4)$$

In order to have a positive $\Re\{Y_{21}\}$, $|\arg\{Y_{21}\}| \leq 90^\circ$. This provides a necessary condition for the mutual coupling between the antennas to be nullified by a practically realizable lumped element network: phase of S_{21} , $\theta = \arg\{S_{21}\}$, should lie in the range $90^\circ \leq \theta \leq 270^\circ$. The phase condition is achieved using transmission lines of the corresponding length at the desired frequency connected to the antenna feeds. The phase condition therefore yields negative $\Re\{-Y_{21}\}$ that can be nullified with a resistive component. On the other hand, $\Im\{-Y_{21}\}$ is either inductive or capacitive on different sides of the centre frequency, making it possible to cancel them by inductive/capacitive elements. Fulfilling the phase condition therefore suffices wideband isolation using reactive and resistive components compared to using only reactive elements.

The main challenge in this method is that, as the spacing between the antennas increases, the derivative, i.e., the slope of $\arg\{Y_{21}\}$ also increases with respect to the frequency. This slope limits the bandwidth over which the given isolation level can be achieved. The value of $\arg\{Y_{21}\}$ can be freely selected as long as the mutual admittance can be cancelled within the input matching bandwidth. The transmission lines used at the input of the antennas also affect the achieved isolation bandwidth as they make the phase slope steeper.

Fig. 3 shows the antenna array with the connected cancellation circuit, i.e., $Y_P = Y_{21}$. The addition of the cancellation circuit introduces resistive losses due to the resistive component of Y_P , G , as well as degrades the input matching of both the antennas. The degradation of the input matching depends on the original isolation between the antennas; with larger natural isolation, Y_{21} is smaller, and hence, addition of a parallel

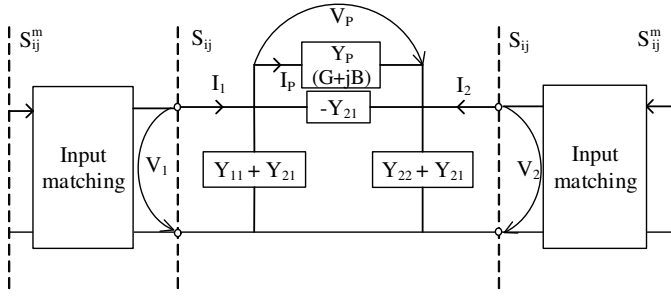


Fig. 3. Schematic of a two-port network with a decoupling circuit.

element will not affect the input matching significantly. The vertical dashed lines in Fig. 3 shows the reference planes for the S parameters of the antenna, with S_{ij} referring to that of the antenna with the additional component for isolation improvement, including the transmission lines at the antenna inputs; S_{ij}^m refers to the S parameters of the entire antenna system including the additional matching and decoupling circuits. Ideally, when $Y_{21} = 0$, i.e., with infinite isolation after the addition of the decoupling circuit, the matching circuits at the two ports are independent of each other. In practice, however, the isolation is always finite and impacts the input matching of the entire antenna system. Conversely, tuning the input matching of the antenna system changes their isolation. It is therefore necessary to design the matching and decoupling circuitries simultaneously.

Furthermore, as the original isolation increases, Y_{21} decreases, resulting in very small values of Y_P . When only reactive elements are used for the decoupling circuit, the component values can be too large or small for implementation, whereas the usage of a resistive element is beneficial as small value of $\Re\{Y_P\}$ results in large resistance values which are easily implementable. This can provide additional narrow band isolation which is required for FDX applications. The proposed decoupling method can be further extended to antenna arrays with more than two elements. However, the extension is subject to significant increase of circuit complexity and hence is beyond the scope of this paper; similar theoretical framework has been presented by other authors, e.g., [11].

B. Impact on efficiency

Using lossy elements in the decoupling circuit may decrease the total efficiency of the antenna. Power is dissipated across the resistive element in addition to the power coupled to the other antenna ports which depends on the isolation achieved with the proposed decoupling circuit. In this subsection, the impact of the resistive element on the efficiency is analysed.

Let us consider a two port network with a lossy parallel element connected between the two ports, i.e., $Y_P = G + jB$ as shown in Fig. 3. Consider a voltage V_1 applied across port 1 with port 2 terminated with the characteristic impedance Z_0 (admittance Y_0). Let I_1 , I_2 and I_P represent the currents in two branches and through the parallel element respectively. The power fed to the antenna at port 1 is $P_1 = \Re\{V_1 I_1^*\}$ where $*$ denotes a complex conjugate. The power lost in the resistive component of the parallel element Y_P is $P_R = \Re\{Y_P^*\} |V_P|^2$.

The loss factor that decreases the efficiency due to the resistive element is given by

$$L_{\text{res-loss}} = \frac{P_R}{P_1} = \frac{\Re\{Y_P^*\} |V_P|^2}{\Re\{V_1 I_1^*\}}. \quad (5)$$

Having derived the voltages and currents at the input to the antenna, the expansion of Eq. (5) yields

$$L_{\text{res-loss}} = \frac{\Re\{Y_P^*\} \frac{|(Y_{22} + Y_0 + Y_{21})|^2 |I_1|^2}{|\Delta|^2}}{\Re\left\{\frac{(Y_{22} + Y_P + Y_0) I_1}{\Delta} I_1^*\right\}}, \quad (6)$$

where

$$\Delta = (Y_{11} + Y_{21})(Y_{22} + Y_{21} + Y_0) - (Y_{21} - Y_P)^2. \quad (7)$$

Expanding Eq. (6) further,

$$L_{\text{res-loss}} = \frac{\Re\{Y_P^*\} \frac{|(Y_{22} + Y_0 + Y_{21})|^2}{|(Y_{11} + Y_{21})(Y_{22} + Y_P + Y_0) - (Y_{21} - Y_P)^2|^2}}{\Re\left\{\frac{(Y_{22} + Y_{21} + Y_0)}{(Y_{11} + Y_{21})(Y_{22} + Y_P + Y_0) - (Y_{21} - Y_P)^2}\right\}}. \quad (8)$$

In order to provide a simplified formula of (8) for calculating the degradation in efficiency, we assume that 1) the two antennas are perfectly matched before the addition of the decoupling circuit i.e. $Y_{11} = Y_{22} = Y_0$, 2) the mutual admittance Y_{21} is purely real at the centre frequency due to the additional transmission lines at the input of the antenna feeds and 3) $Y_{21} = Y_P$. Eq. (8) is then simplified as,

$$L_{\text{res-loss}} \approx \left| \frac{\Re\{Y_{21}^*\}}{(Y_0 + Y_{21})^*} \right|. \quad (9)$$

From [23], we know that $Y_{21} \approx -2Y_0 S_{21}$. Thus, Eq. (9) can be rewritten as

$$L_{\text{res-loss}} \approx \left| \frac{2\Re\{-S_{21}^*\}}{(1 - 2S_{21}^*)} \right|. \quad (10)$$

The efficiency of the entire antenna system including the decoupling and matching circuits can then be described as

$$\eta = 1 - |S_{11}^m|^2 - |S_{21}^m|^2 - L_{\text{res-loss}}, \quad (11)$$

where S_{11}^m and S_{21}^m denote the reflection coefficient and coupling between the antenna ports respectively when the antenna inputs are matched at the resonant frequency after adding Y_P . Eq. (11) does not consider the losses in the antenna itself. When there are no resistive elements connected in Y_P , the isolation as well as the radiated power and efficiency are improved. When a resistive element is connected between the antenna feeds, some power is dissipated in the resistor and the rest is radiated by the antenna. In general, poor original isolation between the antennas decreases the efficiency as power is dissipated in the other antenna ports. Here, original isolation refers to the isolation between two antennas without any decoupling circuits or other isolation improvement techniques. Thus, depending on the value of the resistive element, the efficiency can also be improved if the losses in the resistive element is smaller than the improvement in isolation.

Fig. 4 shows the loss factor $L_{\text{res-loss}}$ due to the addition of a resistance for $\arg\{S_{21}\} = -120^\circ, 135^\circ$ and 180° based on Eq. (6). The figure shows that the use of a purely resistive element for compensating for $\arg\{S_{21}\} = 180^\circ$ results in

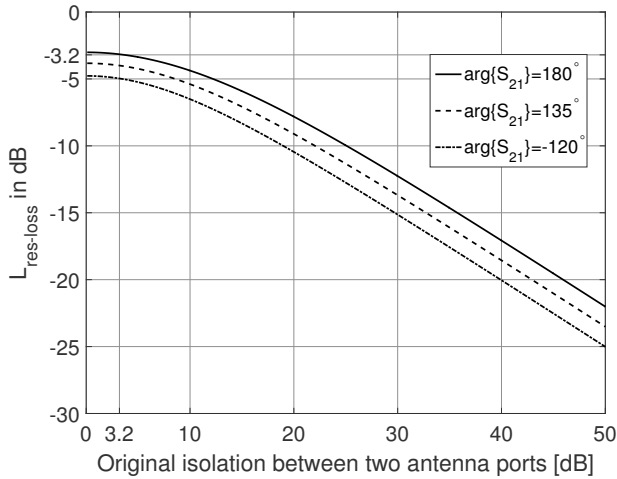


Fig. 4. Loss factor $L_{\text{res-loss}}$ as a function of original isolation for different phases, $\arg\{S_{21}\}$, using a resistor in the decoupling circuit.

larger losses than for $\arg\{S_{21}\} = -120^\circ, 135^\circ$ where the decoupling circuitry is resistive and reactive and $\Re\{Y_{21}\}$ is smaller. In concrete, it is observed from Fig. 4 that applying the decoupling circuit to very closely spaced antennas with strong mutual coupling can improve the efficiency as power is otherwise lost in the coupled antenna port. For example, with the $\arg\{S_{21}\} = 180^\circ$ case, when the original isolation is less than 3.2 dB, the power that the decoupling circuit prevented from coupling to the another antenna is greater than the power is lost in the resistive element of the circuit, thus improving the efficiency. When the isolation is larger than this, there is a decrease in efficiency by appending the decoupling circuit, which would result in a slight decrease in the gain. For example, according to Fig. 4, 10% decrease of the efficiency is expected when the original isolation is 25 dB.

III. SIMULATION AND ANALYSIS

A. Simulation methodology

In order to validate the proposed decoupling method, we consider an antenna array consisting of two closely spaced monopoles operating at 2.4 GHz. Fig. 5 shows the general schematic of the proposed decoupling circuit configuration. The dashed box indicates the decoupling circuit with the transmission lines at the input with length l_a and corresponding phase shift ϕ_a at the design frequency. The three reference planes Π^A , Π^T and Π^M refer to the planes with only antenna, antenna with transmission lines at the input and the complete structure comprising of antenna, decoupling and matching elements respectively. The decoupling circuit comprises of a parallel combination of a resistive and a reactive element (R_P and X_P). The dotted boxes indicate the additional matching components connected at the input of the two ports (X_C and X_S). If the two antennas are symmetric, then the matching components at both antenna feeds can be the same. A simple L-section matching network is indicated in the schematic, although other configurations can be used to improve the matching bandwidth. In order to validate the proposed technique, three different prototypes of closely spaced monopole

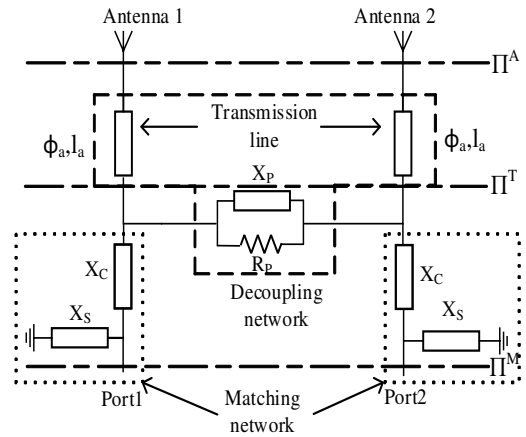


Fig. 5. Schematic of proposed decoupling network configuration showing the decoupling and matching network at the input of the antenna feeds.

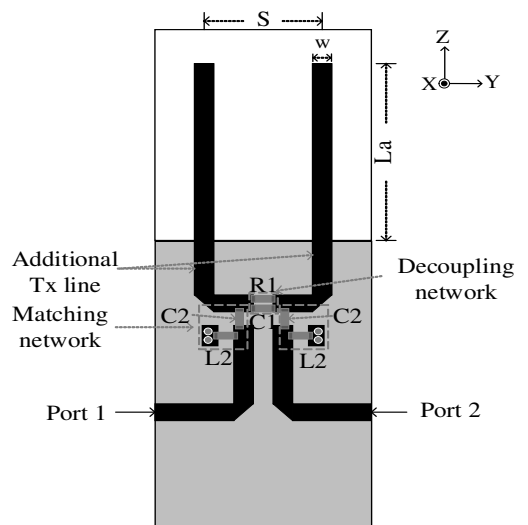


Fig. 6. Schematic of two closely spaced monopoles. Note: The length and shape of the transmission lines shown in the schematic is indicative and differs for each prototype.

antennas are designed with different transmission line lengths at the input. The transmission line transforms the mutual admittance between the two antennas to resistive, resistive and inductive, and resistive and capacitive. The corresponding decoupling circuits are then added to the transmission lines. The prototypes are compared with a reference prototype which consists of the two closely spaced monopoles without any decoupling circuit.

Two closely spaced monopoles adopted from [8] were used to validate the results. First, Ansoft HFSS was used to determine the initial S parameters without matching and decoupling circuitries. The antenna is designed on FR-4 substrate with relative permittivity $\epsilon_r = 4.2$ and a thickness of 0.8 mm. The ground plane on the back side of the two monopole antennas was removed. The antennas are spaced $S = 8.5$ mm apart and printed with a strip width of $w = 1.5$ mm and length $L_a = 21.5$ mm. The overall dimensions of the implemented antenna array is 68×22 mm.

Fig. 6 shows the schematic of the complete antenna system,

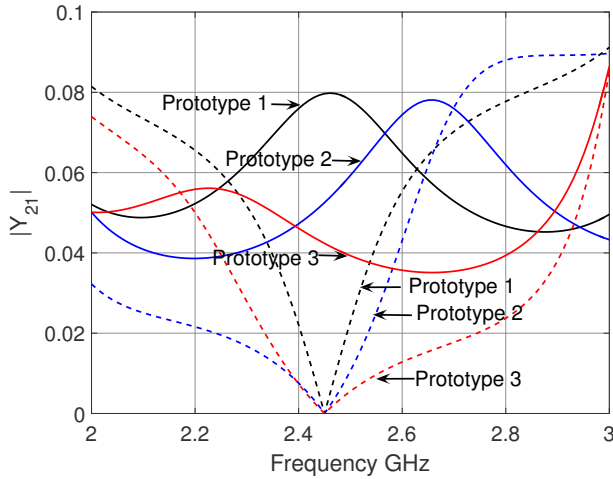


Fig. 7. Simulated mutual admittance between two closely spaced monopoles for the three different cases with $\arg\{Y_{21}\} = 0, -45^\circ$ and 60° . The solid and dashed curves indicate the mutual admittance before and after the addition of a decoupling network along with suitable transmission lines. Smaller values of the admittance indicate improved isolation.

including the monopoles, transmission lines, and the decoupling and matching circuits. Additional transmission lines at the input of the antennas are fabricated as microstrip lines backed by a ground plane. Then, a circuit simulator, Agilent ADS is used to design additional transmission lines to provide the corresponding phase shift at the centre frequency. The length of the transmission lines are then optimized based of full-wave electromagnetic simulations to provide the necessary phase shift. In this work, three different prototypes are analysed such that $\arg\{S_{21}\} \approx 180^\circ, 135^\circ, -120^\circ$, which corresponds to $\arg\{Y_{21}\} = 0^\circ, -45^\circ, 60^\circ$. This fulfills the necessary conditions as described in Section II-A that $\Re\{Y_{21}\}$ can be cancelled in the desired frequency band with the decoupling circuit. For the three different prototypes, the length of the transmission lines are 15.35 mm, 13.70 mm and 17.65 mm corresponding to $\arg\{Y_{21}\} = 0, -45^\circ, 60^\circ$ respectively. The lumped elements $R1$ and $C1$ are connected between the transmission lines which correspond to R_P and X_P respectively in Fig. 5. A simple L-section matching network is connected at the junction to the decoupling circuits so that the antenna array maintains sufficient matching over the band of interest. The components $C2$ and $L2$ correspond to X_C and X_S in Fig. 5 respectively.

Fig. 7 shows the ideal simulated $|Y_{21}|$ of the three prototypes when the resistive and reactive elements are added at plane Π^T in Fig. 5 as the decoupling circuit for the different transmission line lengths. The solid and dashed curves represent $|Y_{21}|$ before and after addition of the decoupling circuit respectively. It shows varying performance of wideband isolation improvement for each prototype. The $|Y_{21}|$ is smaller for Prototypes 2 and 3 compared to Prototype 1 across a wider bandwidth, which proposes that they will achieve more wideband isolation compared to Prototype 1, where mutual admittance is purely resistive. In the considered compact monopole array, the antennas are strongly coupled and hence $|Y_{21}|$ is large.

TABLE II
COMPONENT VALUES FOR DIFFERENT PROTOTYPES.

Component Prototype	Decoupling elements		Matching elements	
	$R1$ (Ω)	$C1$ (pF)	$C2$ (pF)	$L2$ (nH)
1	45	1.6	2.7	0.8
2	68	1.5	3.3	1.1
3	18	0.8	2	0.6

This requires large Y_P for proper decoupling, which adversely affects the input matching. Hence, the antennas are rematched to the centre frequency using a simple L-section matching network at the input.

Based on the simulations, the lumped-component values in the decoupling and matching circuits are selected according to commercially available chip capacitors/ inductors and resistors that provide the highest decoupling and sufficient matching performance of the closely spaced monopole array near the centre frequency. The S parameter models of the components provided by the manufacturer are used in the final simulations. The component values are listed in Table II.

The design procedure followed is summarized as below:

- 1) Full-wave simulation of the antenna array to obtain the S parameters before the addition of the decoupling network.
- 2) Calculation of the required transmission line length based on the approximate formula, Eq. (4) in Section II. The length is then optimized iteratively to achieve the desired Y_{21} phase based on full-wave simulations to account for coupling effects. Since both resistive and reactive elements are used for decoupling, minor changes in the length can be compensated with the lumped component values.
- 3) After the addition of the matching network, circuit optimization is performed to adjust the element values to find the optimal values from both matching and isolation point of view. Ideal components are first used in the simulations in Steps 2 and 3.
- 4) The ideal components are then replaced by component models provided by vendors which may change the achieved decoupling level and frequency band. In this case, the component values are adjusted based on optimization. Finally, full-wave simulation is performed using the S parameters provided by the manufacturer for the selected component values before manufacturing the antenna.

B. Simulation results

Fig. 8(a) shows the simulated input matching of the antennas at plane Π^M in Fig. 5. Since the antenna system is symmetric, the matching of the two ports shows exactly the same trend. The matching bandwidth is smaller for the three prototypes than that of the reference prototype, as it is limited by the additional matching circuitry in the three prototypes. The simulated -10 dB and -6 dB input matching of the antennas is at least 220 MHz and 575 MHz respectively in the operating frequency band. Fig. 8(b) shows the simulated

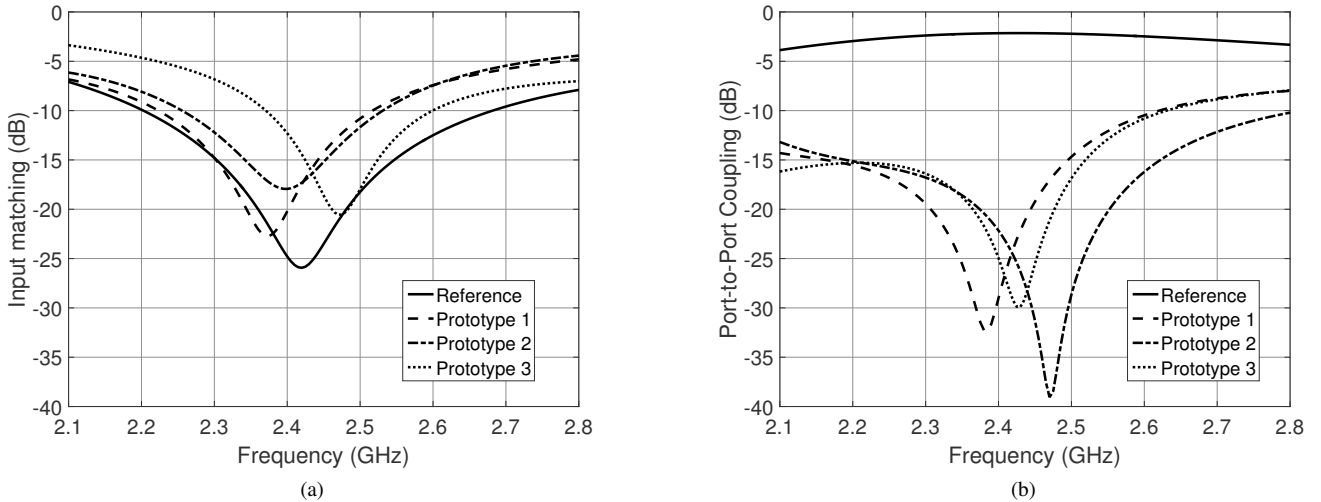


Fig. 8. Simulated S parameters of the antenna prototypes (a) Input matching and (b) Port-to-port coupling. The solid curve shows the input matching and isolation of the reference prototype. The simulated input matching of Port 1 and Port 2 are the same.

port-to-port isolation between the two closely spaced antennas. The proposed technique improves the isolation across at least 330 MHz bandwidth with 15 dB isolation, which corresponds to 13.8% relative bandwidth. Isolation of 30 dB is achievable across 50 MHz bandwidth for Prototype 2 which corresponds to 2% relative bandwidth at 2.4 GHz.

IV. MEASUREMENTS

A. Input matching and isolation

Based on the simulations, the prototypes were manufactured on printed FR-4 substrate, and the lumped components for the decoupling and matching circuit were soldered as shown in Fig. 9. Figs. 10 and 11 show the simulated and measured isolation and input matching of the three prototypes respectively at plane Π^M in Fig. 5. Also, the measured input matching of the reference prototype is shown in Fig. 12. The measured isolation for the three prototypes are similar to the simulation results. The simulated and measured input matching and isolation bandwidths for the different prototypes are compared in Table III. The input matching curves of both antenna ports are very similar to each other in theory. However, there is a small difference in the measured input matching of the two ports which can be attributed to the component tolerances. The measurements confirm the simulation results and show best case isolation of 35 dB across 55 MHz bandwidth at 2.45 GHz for Prototype 2. Considering the original isolation of 2.5 dB, the decoupling network realized an isolation improvement of 32.5 dB in the selected frequency band. The isolation bandwidths for Prototypes 2 and 3 with 15 dB isolation are larger than that of Prototype 1 as shown in Table III. This is due to the phase condition $\arg\{Y_{21}\} = 0$ for Prototype 1 which results in non-zero capacitive or inductive mutual admittance on either side of the design frequency as described in Section II-A which cannot be cancelled by a single reactive element over the desired band. The matching circuitry added along with the decoupling network affected the isolation bandwidth

TABLE III
INPUT MATCHING AND ISOLATION BANDWIDTHS OF THE THREE PROTOTYPES AS WELL AS THE REFERENCE DESIGN AROUND 2.4 GHz.

Level	Matching BW (MHz)		Isolation BW (MHz)			
	-10 dB		15 dB		20 dB	
	Sim.	Meas.	Sim.	Meas.	Sim.	Meas.
Reference	475	375	0	0	0	0
1	290	330	330	370	130	165
2	270	330	425	455	175	190
3	220	215	515	500	110	140

of Prototype 3 most, leading to the lowest bandwidth for the 20 dB isolation level. Among the three prototypes, the least relative bandwidth is 15.4% for 15 dB isolation and 5.8% for 20 dB isolation. This is still better than the ones obtained using only reactive elements in [8], [9] with 1.1% and 5.1% respectively as shown in Table I. Thus, setting $\Re\{Y_{21}\} > 0$ for the frequency band of interest realizes greater isolation bandwidth than the existing technique [8], where Y_{21} is purely reactive at the centre frequency. The new design goal of Y_{21} enables its cancellation using a decoupling circuitry consisting of both resistive and reactive elements.

B. Radiation patterns

The 2D radiation patterns of the designed prototypes were measured in a large anechoic chamber in the azimuth, i.e., XY plane and elevation, XZ plane planes, where the coordinate system is defined in Fig. 6. Fig. 13 shows the azimuth plot of the embedded pattern for the two ports, i.e., during measuring one port, the other port was terminated with 50 Ω load. The radiation pattern is measured using a dual-polarized horn antenna as transmitter and the antenna array as the receiver. A standard dipole antenna with known gain operating at 2450 MHz is also measured with the same measurement setup to calculate the gain of the measured antennas. Fig. 13 shows that the radiation patterns on the azimuth plane are

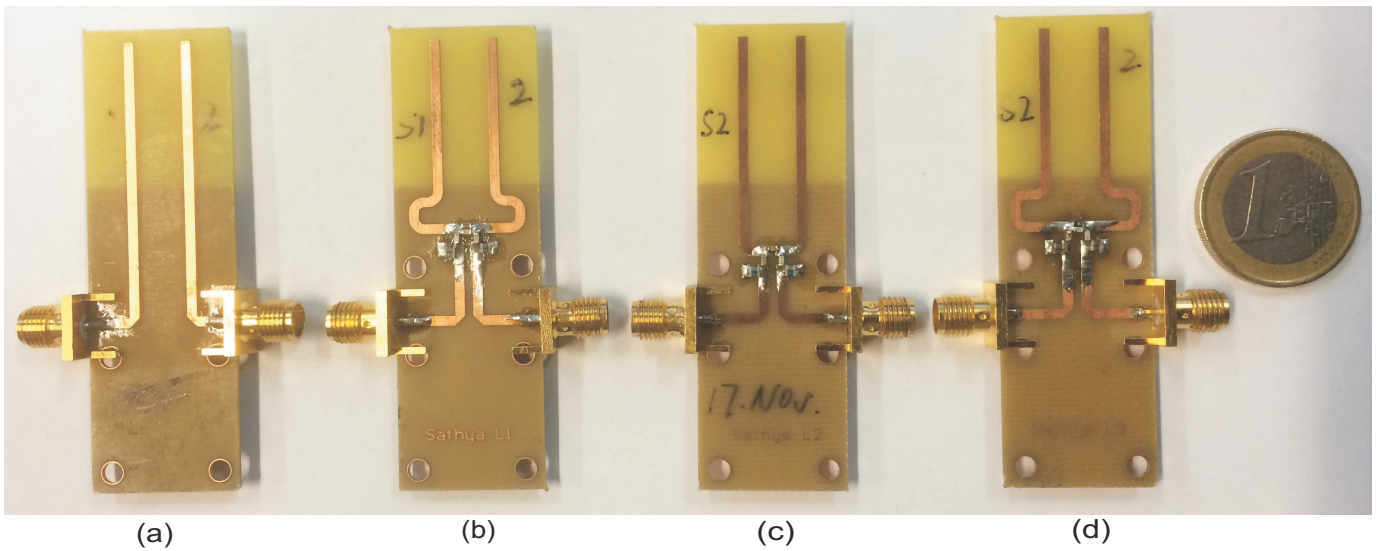


Fig. 9. Photo of all manufactured prototypes (a) Reference (b) Prototype 1 (c) Prototype 2 and (d) Prototype 3.

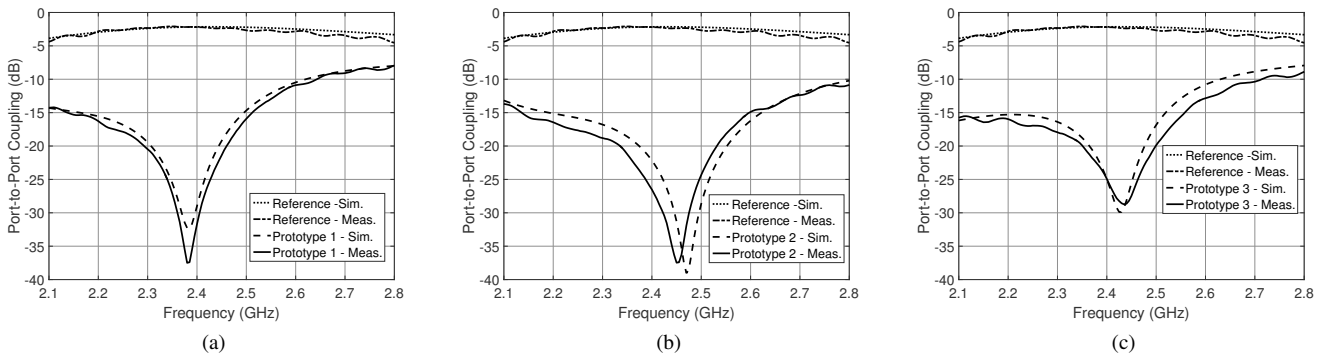


Fig. 10. Measured and simulated port-to-port isolation for the three prototypes (a) Prototype 1, (b) Prototype 2 and (c) Prototype 3. The solid and dashed curve indicates the measured and simulated isolation of the prototypes respectively.

omni-directional. The peak gain of the reference monopole is -5.6 dBi. With use of the decoupling networks, the gain is 1.4 dB better, namely -3.2 dBi for Prototypes 1 and 2 and 4 dB better, namely -1.6 dBi for Prototype 3. The increase in gain is due to reduced coupling that is translated as gain. The power dissipated across the resistor of the decoupling circuit is included. Fig. 14 shows the radiation pattern of the antenna array on the elevation plane. The peak gain is at 0° elevation, i.e., in the azimuth plane. The results demonstrate that the use of resistive elements in the decoupling circuit improves the gain of the antenna without significantly altering the radiation patterns.

C. Efficiency

Fig. 15 shows the efficiency of the measured prototypes based on Eq. (11). The efficiency includes the matching and coupling losses obtained from the measured S parameters of the reference antenna and three prototypes. The resistive loss in the decoupling circuit of the three prototypes ($L_{\text{res-loss}}$ defined in Eq. (8)) is derived from full-wave simulation of the decoupling circuit and circuit models of lumped-components

provided by the manufacturer. The total efficiency does not include the losses of the antenna structure as defined in Eq. (11). Fig. 15 shows that the efficiency of all the three prototypes is between -2.4 dB to -2.8 dB at 2.4 GHz. This corresponds to an improvement of approximately 1.3 dB to 1.7 dB over the reference prototype, which is translated to the antenna gain. Thus, by cancelling the mutual coupling even when using resistive elements, the efficiency can be improved compared to the original case.

V. CONCLUSION

A novel antenna decoupling method for compact arrays suitable for MIMO and FDX applications has been proposed. The paper shows that the proposed decoupling technique improves wideband isolation compared to using only lossless (reactive) or only resistive elements. The wideband isolation was improved by 17.6 dB across a 200 MHz band at 2.4 GHz, with a final isolation level of 20 dB over that band. Over a narrower band of 55 MHz, the isolation was as much as 30 dB corresponding to 2% relative bandwidth which is good enough to implement in-band full-duplex communications in

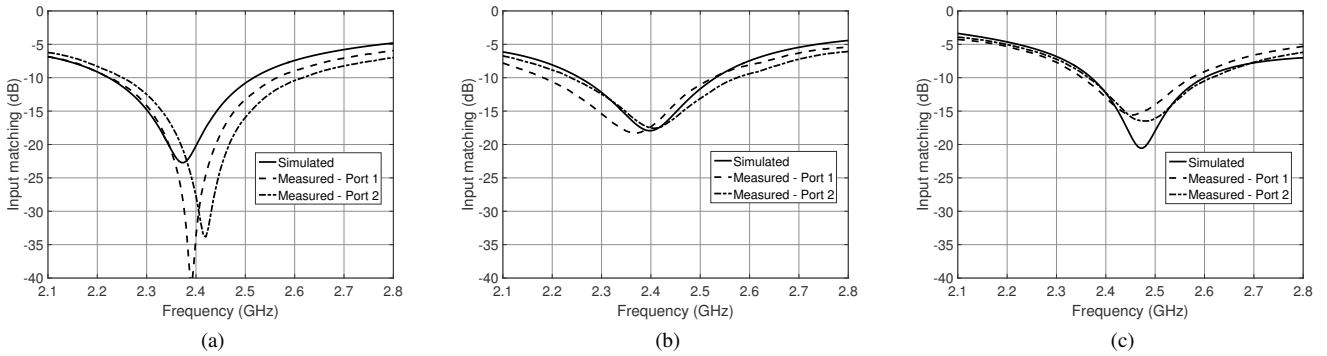


Fig. 11. Measured and simulated input matching for the three prototypes (a) Prototype 1, (b) Prototype 2 and (c) Prototype 3. The solid curve shows the simulated input matching for both ports.

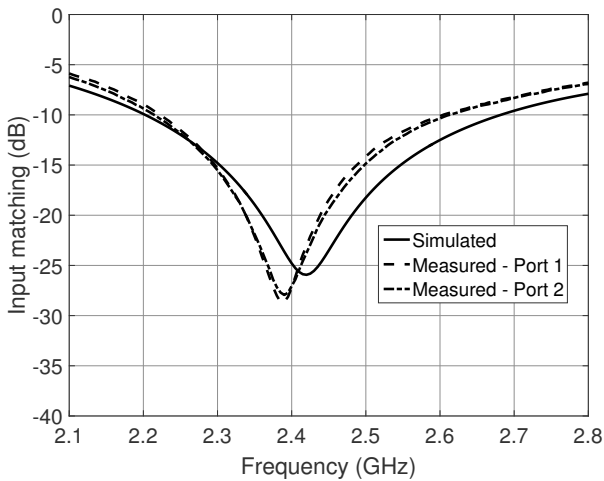


Fig. 12. Measured and simulated input matching for the reference prototype. The solid curve shows the simulated input matching for both ports.

very compact devices. The decoupling circuit comprises of resistive elements along with reactive elements connected in between the antenna feeds. This decoupling circuit affects only the odd-mode impedance of the antennas, while improving the wideband isolation of the closely spaced antenna array. For the monopole configuration, the use of a resistive element improves the isolation, and even though some of the coupled power is dissipated across the resistor, it does not adversely affect the efficiency.

REFERENCES

- [1] R. Vaughan *et al.*, "Antenna diversity in mobile communications," *IEEE Trans. Veh. Technol.*, vol. 36, no. 4, pp. 149–172, Nov 1987.
- [2] A. Sabharwal *et al.*, "In-band full-duplex wireless: Challenges and opportunities," *IEEE J. Sel. Areas Commun.*, vol. 32, no. 9, pp. 1637–1652, Sept 2014.
- [3] M. Heino *et al.*, "Recent advances in antenna design and interference cancellation algorithms for in-band full-duplex relays," *accepted for publication in IEEE Communications Magazine*.
- [4] D. Bharadia *et al.*, "Full duplex radios," *SIGCOMM Comput. Commun. Rev.*, vol. 43, no. 4, pp. 375–386, Aug. 2013.
- [5] T. Husari *et al.*, "Wideband self-adaptive RF cancellation circuit for full-duplex radio: Operating principle and measurements," in *2015 IEEE 81st Vehicular Technology Conf. (VTC Spring)*, May 2015, pp. 1–7.

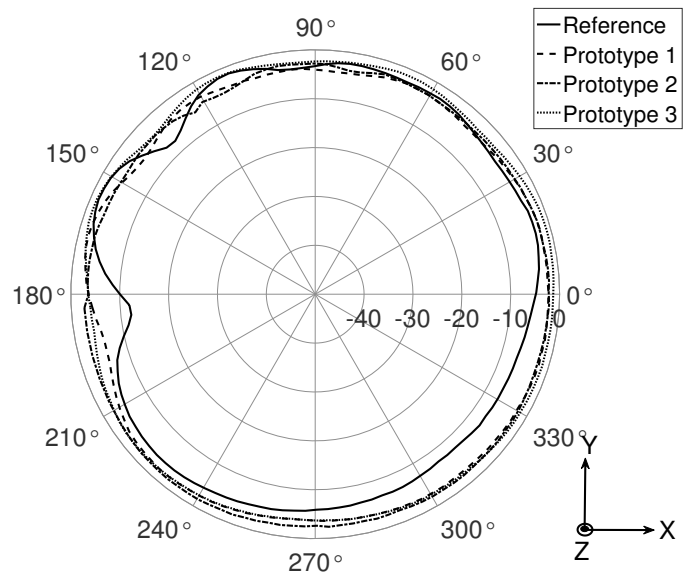


Fig. 13. Measured azimuth radiation pattern for the prototypes with Port 1 excited. During the measurement of each port, the other port was terminated with 50Ω load. The azimuth radiation pattern when Port 2 is excited is similar to that Port 1.

- [6] L. Zhao *et al.*, "A coupled resonator decoupling network for two-element compact antenna arrays in mobile terminals," *IEEE Trans. Antennas Propag.*, vol. 62, no. 5, pp. 2767–2776, 2014.
- [7] A. Diallo *et al.*, "Study and reduction of the mutual coupling between two mobile phone PIFAs operating in the DCS1800 and UMTS bands," *IEEE Trans. Antennas Propag.*, vol. 54, no. 11, pp. 3063–3074, Nov 2006.
- [8] S.-C. Chen *et al.*, "A decoupling technique for increasing the port isolation between two strongly coupled antennas," *IEEE Trans. Antennas and Propag.*, vol. 56, no. 12, pp. 3650–3658, 2008.
- [9] C.-H. Wu *et al.*, "Stub-loaded reactive decoupling network for two-element array using even-odd analysis," *IEEE Antennas Wireless Propag. Lett.*, vol. 12, pp. 452–455, 2013.
- [10] R.-A. Bhatti *et al.*, "Compact antenna array with port decoupling for LTE-standardized mobile phones," *IEEE Antennas Wireless Propag. Lett.*, vol. 8, pp. 1430–1433, 2009.
- [11] H. Chaloupka *et al.*, "Performance enhancement of smart antennas with reduced element spacing," in *2003 IEEE Wireless Communications and Networking, 2003. WCNC 2003.*, vol. 1, March 2003, pp. 425–430.
- [12] J. Coetzee *et al.*, "Port decoupling for small arrays by means of an eigenmode feed network," *IEEE Trans. Antennas Propag.*, vol. 56, no. 6, pp. 1587–1593, June 2008.
- [13] —, "Design of decoupling networks for circulant symmetric antenna

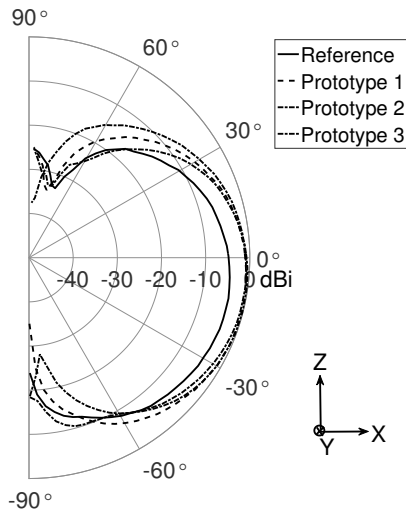


Fig. 14. Radiation pattern of the measured prototypes in the elevation plane.

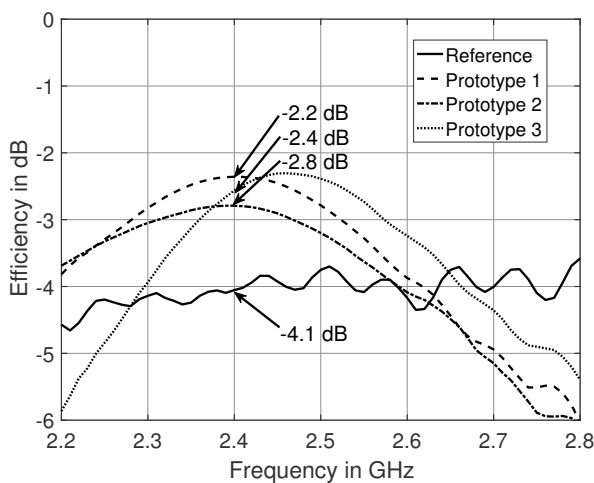


Fig. 15. Calculated total efficiency for the three prototypes (excluding the losses of the antenna structure) derived from measured S parameters along with full-wave simulation of the decoupling circuit and circuit models of lumped-components provided by the manufacturer.

arrays," *IEEE Antennas Wireless Propag. Lett.*, vol. 8, pp. 291–294, 2009.

- [14] X. Tang *et al.*, "Tunable decoupling and matching network for diversity enhancement of closely spaced antennas," *IEEE Antennas Wireless Propag. Lett.*, vol. 11, pp. 268–271, 2012.
- [15] K. Wang *et al.*, "Comparison of compact monopole antenna arrays with eigenmode excitation and multipoint conjugate matching," *IEEE Trans. Antennas Propag.*, vol. 61, no. 8, pp. 4054–4062, Aug 2013.
- [16] S. Chaudhury *et al.*, "Multipoint antenna systems for MIMO and diversity," in *2010 Proc. 4th European Conf. Antennas and Propagation (EuCAP)*, April 2010, pp. 1–5.
- [17] X. Tang *et al.*, "Dual-band decoupling and matching network design for very closely spaced antennas," in *2012 42nd European Microwave Conference (EuMC)*, Oct 2012, pp. 49–52.
- [18] A. Krewski *et al.*, "Matching network synthesis for mobile MIMO antennas based on minimization of the total multi-port reflectance," in *2011 Loughborough Antennas and Propagation Conf. (LAPC)*, Nov 2011, pp. 1–4.
- [19] M. M. Albannay *et al.*, "Dual-frequency decoupling for two distinct antennas," *IEEE Antennas Wireless Propag. Lett.*, vol. 11, pp. 1315–1318, 2012.
- [20] H. Sato *et al.*, "A method of dualfrequency decoupling for two-element mimo antenna," in *Progress in Electromagnetics Research Symp. Proc., (Stockholm)*, 2013, pp. 1853–1857.

- [21] A. Mak *et al.*, "Isolation enhancement between two closely packed antennas," *IEEE Trans. Antennas Propag.*, vol. 56, no. 11, pp. 3411–3419, Nov 2008.
- [22] R. Valkonen *et al.*, "Determining bandwidth estimators and matching circuits for evaluation of chassis antennas," *IEEE Trans. Antennas Propag.*, vol. 63, no. 9, pp. 4111–4120, Sept 2015.
- [23] S. N. Venkatasubramanian *et al.*, "On the constraints to isolation improvement in Multi-Antenna systems," in *9th European Conf. Antennas and Propagation (EuCAP 2015)*, Lisbon, Portugal, Apr. 2015.
- [24] J. Reed *et al.*, "A method of analysis of symmetrical four-port networks," *IRE Trans. Microw. Theory Techn.*, vol. 4, no. 4, pp. 246–252, October 1956.
- [25] J.-S. Hong *et al.*, *Microstrip Filters for RF / Microwave Applications*. Hoboken, US: Wiley, 20101213 2010.
- [26] C. Wu *et al.*, "Very compact fully lumped decoupling network for a coupled two-element array," *IEEE Antennas Wireless Propag. Lett.*, vol. 15, pp. 158–161, 2016.



Sathya N. Venkatasubramanian received the M.Sc. (Tech.) degree in radio science and engineering from Aalto University, Espoo, Finland, in 2013. Since 2013, he is pursuing the Doctoral degree at the Department of Radio Science and Engineering, Aalto University School of Electrical Engineering, Espoo, Finland. His research interests include antennas and propagation for in-band full-duplex systems.



Linsheng Li (S09-M14) received the B.Eng. in information engineering and PhD. in electrical engineering from Southeast University (SEU), Nanjing, China, in 2007 and 2014, respectively. During Sep. 2014 to Jul. 2016, he was with the department of radio science and engineering, Aalto University in Finland as a research engineer. Since Aug. 2016 he is with the research center of Huawei in Helsinki as an antenna designer. His current research interests include millimeter wave antennas for mobile terminals for 5G and future wireless communication.



Anu Lehtovuori received the M.Sc. (Tech.) and Lic.Sc. (Tech.) degrees in electrical engineering from Helsinki University of Technology, Espoo, Finland, in 2000 and 2003, respectively, and D.Sc. (Tech.) degree in electrical engineering from Aalto University, Espoo, Finland, in 2015. From 2004, she has been a University Teacher with Helsinki University of Technology and currently with Aalto University School of Electrical Engineering, Finland. Her research interests include circuit simulation, engineering education, handset antennas, and especially circuit elements in antenna design.



Clemens Icheln received the M.Sc. degree in Electrical Engineering (Dipl.-Ing.) at Hamburg-Harburg University of Technology, Germany, in 1996, the Licentiate degree in Radio Engineering and the Doctor of Science in Technology degree at Helsinki University of Technology, Finland, in 1999 and 2001, respectively. He is currently working as University Lecturer at the Department of Radio Science and Engineering of Aalto University School of Electrical Engineering. His main research interests are the design of antennas for small communications devices such as mobile terminals and compact relays, and suitable antenna characterisation methods.



Katsuyuki Haneda received the Doctor of Engineering from the Tokyo Institute of Technology, Tokyo, Japan, in 2007. Dr. Haneda is presently an assistant professor in the Aalto University School of Electrical Engineering. He is the recipient of the best paper award of the antennas and propagation track in the IEEE 77th Vehicular Technology Conference (VTC2013-Spring), Dresden, Germany, and of the best propagation paper award in the 7th European Conference on Antennas and Propagation (EuCAP2013), Gothenburg, Sweden. Dr. Haneda has been an associate editor of the IEEE Transactions on Antennas and Propagation between 2012 and 2016, and an editor of the IEEE Transactions on Wireless Communications since 2013. He has also been an active member of a number of European COST Actions, e.g., IC1004 Cooperative radio communications for green smart environments and CA15104 Inclusive Radio Communication Networks for 5G and beyond (IRACON). His current research activity includes high-frequency radios such as millimeter-wave and beyond, wireless for medical, post-disaster scenarios and internet-of-things, and in-band full-duplex radio technologies.